AD-A230 648

REPORT DOCUMENTATION PAGE

Form Approved
OMB No. 0704-0188

1 AGENCY USE ONLY *(Leave blank)*	2 REPORT DATE	3 REPORT TYPE AND DATES COVERED
	December 1990	Professional paper

4 TITLE AND SUBTITLE

LIQUID METAL FUEL COMBUSTION MECHANICS

5 FUNDING NUMBERS

PE: ZW18
WU: DN309 170
PE: 0601152N

6 AUTHOR(S)

T. Duvvuri

7 PERFORMING ORGANIZATION NAME(S) AND ADDRESS(ES)

Naval Ocean Systems Center
San Diego, CA 92152-5000

8 PERFORMING ORGANIZATION REPORT NUMBER

9 SPONSORING/MONITORING AGENCY NAME(S) AND ADDRESS(ES)

Office of Chief of Naval Research
Independent Research Programs (IR)
OCNR-10P
Arlington, VA 22217-5000

10 SPONSORING/MONITORING AGENCY REPORT NUMBER

11 SUPPLEMENTARY NOTES

12a DISTRIBUTION/AVAILABILITY STATEMENT

Approved for public release; distribution is unlimited.

12b DISTRIBUTION CODE

13 ABSTRACT *(Maximum 200 words)*

The modeling of the droplet formation at the gas/liquid boundary interface of a gaseous jet injected into a liquid metal bath and the turbulent mixing of the resultant two-phase (gas/liquid droplets) mixture is presented as a preliminary to the analysis of the liquid metal fuel combustion problem. The model is used to predict velocity and liquid droplet fraction distributions across the mixing zone and along the centerline of the jet. These results show that the distribution of the liquid fuel droplets peaks away from the region of maximum oxidizer concentrations.

Published: *AIAA/SAE/ASME/ASEE*, 26th Joint Propulsion Conference, July 1990

14 SUBJECT TERMS	15 NUMBER OF PAGES
liquid metal fuel	16 PRICE CODE

17 SECURITY CLASSIFICATION OF REPORT	18 SECURITY CLASSIFICATION OF THIS PAGE	19 SECURITY CLASSIFICATION OF ABSTRACT	20 LIMITATION OF ABSTRACT
UNCLASSIFIED	UNCLASSIFIED	UNCLASSIFIED	SAME AS REPORT

AIAA 90-2308

LIQUID METAL FUEL COMBUSTION MECHANICS

TIRUMALESA DUVVURI
Naval Ocean Systems center
San Diego, CA

AIAA/SAE/ASME/ASEE
26th Joint Propulsion Conference
July 16-18, 1990 / Orlando, FL

LIQUID METAL FUEL COMBUSTION MECHANICS

Tirumalesa Duvvuri*
Naval Ocean Systems Center
San Diego, CA 92152-5000

Abstract

The modelling of the droplet formation at the gas/liquid boundary interface of a gaseous jet injected into a liquid metal bath and the turbulent mixing of the resultant two-phase (gas/liquid droplets) mixture is presented as a preliminary to the analysis of the liquid metal fuel combustion problem. The model is used to predict velocity and liquid droplet fraction distributions across the mixing zone and along the centerline of the jet. These results show that the distribution of the liquid fuel droplets peaks away from the region of maximum oxidizer concentrations.

Nomenclature

- a Speed of sound
- B_a Empirical constant for atomization drop size
- C_a Empirical constant for atomization rate
- C_v Specific heat at constant volume
- d Liquid Droplet diameter
- D_k Droplet drag per unit relative velocity
- F Fractional volume of gas
- G Body force
- h Specific Enthalpy
- H Liquid Droplet specific enthalpy
- I Specific internal energy
- K Thermal conductivity
- K_D Turbulence model empirical constant, = O(0.1)
- m Droplet mass
- M_a Mass stripped away at the gas/liquid interface
- $\mathfrak{m}$ Molecular weight
- Nu Nusselt numbert
- p Pressure
- Pr Prandtl number
- r Droplet radius; or radial coordinate
- R Universal gas constant
- Re Reynolds number
- S' Droplet momentum coupling term
- Sc Schmidt number
- S_w Droplet angular momentum coupling term
- t Time
- T Temperature
- u,v,w Gas velocity components
- U,V,W Liquid droplet velocity components
- V_m RMS velocity of gas molecules
- We Weber number
- x Radial or transverse coordinate
- y Axial coordinate
- $\mathcal{E}$ Turbulent kinetic energy level for droplet dispersion
- Λ Cell scale length for turbulence model
- μ Viscosity
- ρ Density
- σ Viscous stress tensor; surface tension
- τ Turbulence scale for droplet dispersion
- ∇ Differential Operator, grad

Subscripts

- d Liquid Droplets
- g Gas
- k Species no., droplet no.
- l Liquid
- r Relative

INTRODUCTION

The impetus for Liquid Metal Fuel Combustion research arose from an interest in finding closed loop high energy density compact propulsors for underwater applications. A Stored Chemical Energy Propulsion System (SCEPS) produced by combining a closed-volume, liquid metal combustor with the boiler of a classical Rankine cycle, shown schematically in Fig. 1, satisfies these requirements.[1-4] Fig.2 shows the schematic of the boiler-reactor, and Figs. 3 and 4 show two types of the metal combustor itself.

In either case a gaseous oxidizer jet is injected (fig.5) into a liquid metal fuel bath in the combustor. As the oxidizer and the fuel are separately introduced, the combustion process in this case is mixing limited. The fundamental mechanisms involved in the combustion process for such a case (gaseous oxidizer jet into a liquid fuel) are not well understood.

Presently available studies analyze the problem under the Locally Homogoneous Flow (*LHF*) approximation.[5-9] These analyses do not consider the important processes that occur at the gas/liquid interface as well as in the mixing region. Namely, (A) the liquid droplet formation, their agglomeration and breakup as well as, (B) the phase changes, (vaporization and condensation), and (C) their effect on the combustion process. (D) Further, the effects of velocity and thermal lags, (between the gaseous phase and liquid droplets), on the turbulent mixing and hence on the efficiency of the (mixing limited) combustion are not known.

It is well known from fuel spray combustion studies for gas turbine combustors,[10-12] that fuel droplet sizes can have direct impact on almost all key aspects of combustion. The initial droplet sizes formed at the injector exit and their trajectories, coupled with the combustor primary zone turbulent mixing significantly influence the evaporation and combustion characteristics of the fuel droplets. The droplet trajectories themselves are influenced by the

---

*Scientist
Associate Fellow AIAA

velocity and thermal lags between the phases. Also the droplet evaporation, ignition and combustion is also dependant on the droplet size distribution (amount of surface available for efficient heat transfer) and its thermal lag (temperature differential between the phases) from surrounding gas.

Previous studies, by the author, of turbulent mixing, ignition and combustion of two phase (gas-solid-particle/pure-gas) flows have shown these velocity/thermal lags to play an important part in the slow down of the spread of the two phase mixture (in particular the solid fuel particles) into the mixing zone[13-15] and thus keeping the center two-phase jet intact to a longer axial length. (This inefficient mixing of the oxidizer and the fuel leads to combustion inefficiencies due to non- optimum oxidizer/fuel mixture ratios.) Similar observations, about longer intact center jet, have been made in recent experimental studies at NOSC by Parnell et al[16]. These studies show "a continuous gaseous jet extending about 60% of the length of the combustion chamber", whereas calculations by LHF aproximation analyses by Lin etal of Pennstate[9], show a much shorter jet core.

The aim of this study is to provide an insight into these fundamental mechanisms. Understanding of these fundamental mechanics of the mixing, ignition and combustion process would aid in designing very efficient propulsion devices. This would also further advance our understanding of the fundamental mechanics of the multi-phase multi-specie turbulent reacting/ combusting flows.

This is a continuing research program and this paper presents the progress to date. As a first step in analyzing this complex problem, the present work considers the turbulent mixing of the two-phase (gas/liquid particle) non-combusting mixture. The work accomplished includes a critical review of previous work, modelling of the number density distribution of the liquid metal fuel droplets generated at the gas/liquid boundary as well as the velocity lag effect between the gaseous and liquid droplet phase. This model was incorporated into fluid flow equations for the turbulent mixing of a two-phase (gas/liquid droplet) mixture. The results of some preliminary calculations are presented and discussed.

THE GOVERNING EQUATIONS

There are three fluid phases that need to be considered in our problem, namely, the gas, the liquid and the droplets. The equations for the gas and liquid are the usual Eulerian continuum fluid dynamic equations augmented by the mass, momentum and energy exchange terms due to the droplet phase. The droplets are treated as discrete particles travelling through the continuum and their dynamic behaviour is described by Lagrangian equations.[19]

For our case where a gaseous jet is injected into a liquid bath, the liquid enters into the picture mainly at the gas/liquid interface where a radial velocity is induced to the fluid due to the entrainment effect of the gaseous jet. The liquid again enters into the picture once the gas jet has dissipated its momentum and subsumed by the liquid or condenses to liquid.

The gaseous phase will be considered to be consisting of a multi-species compressible mixture while the liquid phase will be assumed to be incompressible with a constant density. The mass conservation equation for the two-phase fluid is:

$$\partial\bar{\rho}/\partial t+\frac{1}{r}\nabla.\,(r\bar{\rho}\vec{u}) = \dot{\bar{\rho}}_s \qquad (1)$$

where $\dot{\bar{\rho}}_s$ is the mass of liquid that is stripped away as droplets or as a result of phase change (evaporation or condensation), and

$$\bar{\rho} = F\rho_g + (1-F)\,\rho_l \qquad (2)$$

The gas mixture obeys the summation rules of :

$$\rho_g = \Sigma\rho_k \qquad (3)$$

$$I_g = \Sigma(\rho_k/\rho_g)\,I_k \qquad (4)$$

$$C_v = \Sigma(\rho_k/\rho_g)\,C_{vk} \qquad (5)$$

$$h_g = \Sigma h_k = \Sigma(I_k + RT/\mathfrak{M}_k) \qquad (6)$$

$$p = RT\Sigma(\rho_k/\mathfrak{M}_k) \qquad (7)$$

and the mass conservation equation for species k is given by

$$\frac{\partial\rho_k}{\partial t}+\frac{\vec{u}}{r}.\nabla(r\rho_k)+\frac{1}{r}\frac{\rho_k}{F}\nabla.\,(r\vec{u}) = \frac{1}{r}\nabla.\,(r\rho D\vec{\nabla}\rho_k/\rho_g)+\dot{\rho}_s\delta_{kl} \qquad (8)$$

Summing over all species, the mass conservation equation for the gaseous phase alone is,

$$\frac{\partial\rho_g}{\partial t}+\frac{\vec{u}}{r}.\nabla(r\rho_g)+\frac{1}{r}\frac{\rho_g}{F}\nabla.\,(r\vec{u}) = \dot{\bar{\rho}}_s-\frac{\dot{\rho}_s}{F} \qquad (9)$$

Combining equations 1,2,9, the equation for F is obtained as:

$$\frac{\partial F}{\partial t}+\frac{1}{r}\nabla.\,(r\vec{u}F) = \frac{1}{r}\nabla.\,(r\vec{u}) \qquad (10)$$

The x,y-momentum equations for both the gas and liquid phases are given by

$$\frac{\delta \bar{\rho}\vec{u}}{\delta t} + \frac{1}{r}\nabla.(r\bar{\rho}\vec{u}\vec{u}) = -\nabla p - \frac{(\sigma_o - \bar{\rho}w^2)}{r}\nabla r + S' + \bar{\rho}G \quad (11)$$

where $S' = -\sum D_k/m_k\ (u_g - U_k)$, (D_k being the drag force term defined below), is the droplet momentum coupling term. G is the body force and σ_o is the cylindrical viscous stress given by

$$\sigma_o = (2\frac{\mu_t}{r})\vec{u}.\nabla r \quad (12)$$

μ_t is the turbulent viscosity

$$\mu_t = \frac{\rho}{\sqrt{2}} K_D \Lambda^2 |def u| \quad (13)$$

where $|def\ u|$ is the magnitude of the deformation tensor.

For axisymmetric flow with swirl, the two-dimensional Navier-Stokes equations are supplemented with the angular momentum equation

$$\frac{\delta(r\bar{\rho}w)}{\delta t} + \frac{1}{r}\nabla.(r^2\bar{\rho}w\vec{u}) = \frac{1}{r}\nabla.(r\bar{\tau}) + S_w \quad (14)$$

where

$$\bar{\tau} = \mu r^2 \nabla(\frac{w}{r}) \quad (15)$$

Finally the equation for the internal energy is given by:

$$\frac{\delta(\bar{\rho}\bar{I})}{\delta t} + \frac{1}{r}\nabla.(r\bar{\rho}\bar{I}\vec{u}) = -\frac{p}{r}\nabla.(r\vec{u}) + \bar{\tau}.\nabla(w/r) + \frac{\sigma_o}{r}\vec{u}.\nabla r - 1/r\ \vec{\nabla}.(r\bar{j}) + Q_c + Q_s \quad (16)$$

where the heat flux consists of both conduction and diffusion terms

$$\bar{j} = K\nabla T - \rho_g D \Sigma h_k \nabla(\frac{\rho_k}{\rho_g}) \quad (18)$$

All the source terms in equations 1,10,13 and 15 refer to the production rate per unit total volume $V_g + V_l$ and

$$I = (M_g I_g + M_l I_l)/(M_g + M_l) \quad (19)$$

The Liquid Droplet Phase Equations

The droplets are tracked in a Lagrangian fashion. Thus their mass conservation is given by

$$\frac{dm_k}{dt} = \dot{m}_{evap} \quad (20)$$

where m_{evap} is the mass of droplets evaporated or coalesced or absorbed into the liquid surface.

Momentum conservation is given by:

$$\frac{d\vec{U}_k}{dt} = \frac{D_k}{m_k}(\vec{u} - \vec{U}_k) + \frac{W_k^2}{r}\nabla r + \vec{G}_k \quad (21)$$

where G_k is the body force or buoyancy term. When a swirl component is present, it is given by

$$\frac{dW_k}{dt} = \frac{D_k}{m_k}(w - W_k) - U_k\frac{W_k}{r_k} \quad (22)$$

while the droplet energy conservation is given by

$$m_k\frac{dH_k}{dT} = L(T_k)\frac{dm_k}{dt} + q_k \quad (23)$$

where L_k is the latent heat of vaporization and q_k is the rate of heat transfer to the droplet from the surrounding gas.

Following Duckowicz[19], a Monte Carlo droplet group representation is used, i.e., each droplet parcel actually represents a certain number (can be fractional) of particles of identical characteristics in radius, velocity, temperature etc. Except in the case of very few parcels, this spray is expected to statistically behave like the actual droplet cloud.

These equations for the droplet phase combined with those given earlier for the continuum gas, liquid phases describe the flow fully once the interaction terms of mass, momentum and energy exchange between the droplets and gas/liquid are defined.

LIQUID DROPLET FORMATION

The first problem that will be tackled is the modelling of the liquid droplet formation at the gas/liquid interface. The rate of generation of the number densities of various sizes of liquid droplets at the gas/liquid boundary is modelled by combining the local mass strippping rate formulation of Mayer [17], with the Sauter mean diameter formula of Ingebo [18] along with a probability distribution function (pdf) for size distribution around this mean diameter, as per Dukowicz [19].

Liang etal [20,21] have found that Mayer's atomization theory was quite successful in modelling the liquid fuel spray formation in rocket fuel injectors.

Based on Mayer's theory[17] of capillary wave amplification, this

mass stripping rate $\dot{M}_a$ is given by

$$\dot{M}_a = C_a \left[\frac{\mu_l (\rho_g \epsilon v_r^2)^2}{(\sigma_l/\rho_l)} \right]^{\frac{1}{3}} D_j \delta y \qquad (24)$$

where the constant C_a was found to be between 0.2 and 0.3. v_r is the relative velocity between the gas and liquid at the gas/liquid inerface.

This quantity $\dot{M}_a$ will be equal to the sum of the masses of all the droplets N of diameter d formed at the boundary, namely,

$$\dot{M}_a = \Sigma \rho_l N_d d^3 \qquad (25)$$

where ρ_l is the density of the liquid.

Ingebo (20) has studied the gas density effects on liquid droplet sizes and found that the Sauter mean diameter is given by the formula

$$\frac{d_o}{d_s} = 4.33 \times 10^{-11} (We Re \rho_g)^{0.44} (\rho_l V_m^3 / \mu_g)^{0.75} \qquad (26)$$

where We, Re are the Weber and Reynolds numbers, d_o is the injector orifice diameter and d_s is the Sauter mean diameter defined by $\Sigma nd_i^3 / \Sigma nd_i^2$. V_m is the RMS velocity of the gas molecules.

As for the probability distribution function for the particle sizes, Duckowicz[20] found

$$f_r(r) = \frac{6}{d_s} \exp\left(\frac{-6r}{d_s}\right) \qquad (27)$$

where r=d/2 is the radius of the liquid droplets.

Equations 23-26 can be combined together to determine the number density of a particular droplet size by noting that the number of droplets dN of radius r in the interval dr, located at position x, in the volume interval dx, and with velocity u_p in the interval du_p at time t is given by

$$dN = f(r, x, u_p, t)\, dr dx du_p \qquad (28)$$

However for computational purposes, this function is represented by five distinct groups, with one-fifth of the liquid droplet mass being assigned in random order to each of them. These five ratios of actual size to mean drop size are taken from Ingebo:

$$\frac{d}{d_s} = (0.198, 0.759, 1.0, 1.23, 2.30) \qquad (29)$$

Liquid Droplet Drag

For liquid droplets of molecular size one may assume no velocity lag between the fluid and droplet phases. It is in this appoximation that one has the LHF (Locally Homogeneous Flow) model discussed earlier. However, for liquid droplets of significant size in the flow there will be a velocity lag between the carrier gas and the liquid droplets. The effect of this velocity lag between the gas and liquid droplet is characterized by the momentum coupling term S in equation (11) and the drag force term D_k in equations 20, 21. It is given by

$$D_k = 6\pi\mu r_k + \frac{1}{2\pi} r_k^2 C_D |\vec{u}_r| \qquad (30)$$

here the drag coefficient C_D 's dependance on the Reynolds number is given by

$$\begin{aligned} C_D &= 24\ (Re_d)^{-0.84} && Re_d < 80 \\ &= 0.271\ (Re_d)^{0.217} && 80 < Re_d < 10^4 \\ &= 2. && Re_d < 10^4 \end{aligned} \qquad (31)$$

This variation in the drag coefficient with the Reynolds number approximately accounts for effects of the flattening of the droplet and the resultant increase in drag coefficient as the droplet deforms.

Dispersion of liquid droplets due to turbulence

As discussed by Dukowicz[19], the effects of turbulence on the diffusion of the liquid droplets can be described in two ways. One way is to assume a droplet diffusion equation with a turbulent particle diffusivity. The evaluation of this turbulent particle diffusivity requires turbulence modelling to evaluate the properties of the turbulence field as done by Mostafa and Elghobashi[22].

As discussed by Dukowicz, an alternate possibility (which is adopted in this paper), is to attempt to model the diffusion directly, as a random walk of particles acted on by the turbulent gas velocity field. Assuming isotropy and a Gaussian velocity distribution for the gas turbulence, random instantaneous turbulent velocities for the liquid droplets may be selected from

$$\vec{u} = \vec{u}_{mean} + \vec{e}^{\frac{1}{2}} sgn(X, Y)\, erf^{-1}(|X|, |Y|) \qquad (32)$$

where X and Y are random variables uniformly selected from the range (-1,+1). ϵ is the turbulent kinetic energy level (usually specified as a fraction, say 10%, of the mean flow kinetic energy). This velocity perturbation acts for a duration equal to τ (another empirical parameter), which can be thought of as the time it takes for a typical droplet to traverse the width of a typical turbulent eddy.

The turbulent dispersion of the liquid droplets is thus dependant on the empiricism involved in defining ϵ, τ which need to be evaluated by correlating the predictions of this model to experimental observations.

NUMERICAL SOLUTION

The numerical solution scheme used for the solution of the fluid and droplets equations given above, is a modification and extension of the multi-step ICE-ALE solver code[21,23]. One can refer to them for complete details. Only a few salient features are discussed

below.

The scheme is nominally first order accurate in both space and time. In the time dimension, the scheme is essentially a split time-step marching procedure, evaluating all quantities explicitly using the most updated values of the field variables upto that point in the solution cycle. The only exception is that of solving for the fluid accelerations due to pressure. In view of the strong coupling between the pressure and velocities, the velocity updates are made implicit with pressure, thus overcoming Courant stability restriction.

One of the important questions that arises in analyzing particle-laden flows is that of the evaluation of pressure. For particles of molecular size or in the LHF approximation, the effect of these particles is treated as though it is another species of a certain mass fraction, thus entering into the calculation of the value of density in the gas equation p=o RT. For particles of more significant size where they are treated as a separate phase, their contribution to pressure may be modelled after Statistical Mechanics of continua if they are assumed to have a completely random position and velocity as the molecules in the Classical Statistical Mechanics. No such analysis seem to have been done todate. The other way is to calculate the fluid pressure by excluding the particles in a given volume, thereby reducing the effective areaa over which the pressure is applied. This is the method adopted in our work.

The major steps in the solution procedure are:

Step 1. Explicit lagrangian evaluation of: Liquid Droplet formation and transportation; All gas-droplet coupling terms; All viscous diffusion terms; Pressure gradient and body force updates of velocity

Step 2. Implicit updating of velocities: Point pressure iterative correction for fluid velocities; Implicit coupling of droplet velocities

Step 3. Evaluation of convective terms: Gas & Liquid mass, energy convection; Momentum convection

RESULTS

In this section, the results of some simulations are presented. This code is time-accurate and is suited for modelling transient phenomena. The physical duration of the simulation run is divided into a large number of time-steps or cycles whose size is continually being modified on numerical stabiliity considerations. For fixed boundary conditions, a steady-state solution is obtained by running the problem long enough until all transient effects of the flow field died out.

The principal interest in this phase of the work is to see how well the models predict the fluid properties across the mixing zone and along the combustor centerline, the flow boundaries (Fig.5), the particle boundaries and their velocities. The results presented here are for an oxygen gas jet injected into a liquid hydrogen bath. The injector inner dia is 0.089" and the combustor diameter is 0.62" and is 12" long. The gas jet velocities are varied from 0.6e4 cm/sec to 9.6e4 cm/sec. The results presented are for 200 cycles. The computational grid i*n the combustor is shown in Fig.6.

Figs. 7a, 7b, 7c show the axial velocity distributions across the mixing zone for three jet velocities, 3.57e4, 5.93e4 and 8.11e4 cm/sec respectively. The velocity is normalized by the maximum axial velocity. Each of the figures contains the distributions for several axial locations in the combustor. It is seen from the figures that the maximum axial velocity (V/Vmax=1) is reached downstream of the jet exit plane where the extent of the constant velocity region i.e. the unmixed core of the jet has ben reduced from the maximum (x=11) to (x=2) at an axial locatio of about 7. The velocity distributions are different for different jet exit velocities.

Fig. 8 shows a typical velocity distribution along the combustor centerline. The maximum axial velocity for this case is 5.93e4 cm/sec. The figure shows that the jet accelerates upto about 10 axial locations before peaking up. At about y=25, the jet completely dissipates its momentum and the jet velocity approaches zero.

Figs. 9a, 9b, 9c show the distribution of the liquid fraction F across the mixing zone. F=1.0 means fully gaseous, while F=0.0 means fully liquid and for other values of F in between, part of the cell at that location is liquid and part of it is gas. For the lowest speed of the jet of 3.57e4 cm/sec shown in Fig. 9a, one sees changes in F only towards axial location of y=9. This means that the gas jet is not mixing very much with the surrounding liquid. As the speed of the gas jet increased, Figs. 9b (Vmax=5.93e4 cm/sec), and Fig.9c (Vmax = 8.11e4 cm/sec), the changes in F are seen earlier.

The variation of the liquid fraction F, along the combustor centerline is shown in Figs.10a, 10b. In Fig. 10a with the lower jet speed of 2.35e4 cm/sec, the jet center remains fully gaseous for a longer axial distance than the higher speed, 5.93e4 cm/sec, case of Fig. 10b. This means that the higher jet speed is conducive to more mixing between the gas jet and the surrounding fluid.

Finally the location of the liquid particles within the mixing zone are shown in Fig.11a (Vmax=4.8e4 cm/sec) and Fig.11b (Vmax=3.6e4 cm/sec). In these figures x=0 corresponds to the jet or combustor centerline while y=0.3 corresponds to the combustor face plane. It is seen from the two figures that all the particles are located farther away from the jet centerline and farther downstream along the axis. The particles closest to the centerline, x=0, are farthest along the jet centerline. In other words the particle boundary peaks away from the oxygen rich center region of the gas jet. As discussed earlier, the model for the turbulent dispersion of the liquid droplets contains certain empirical constants, namely, the resident time t and the turbulent kinetic energy fraction. A parametric variation of these variables need to be carried out to get complete picture. It is proposed to do so.

CONCLUSIONS

Models are developped to describe the formation and characteristics (number density/diameter distributins) of liquid droplets at the gas/liquid interface of a gas jet injected into a liquid bath at rest. Their dispersion by the carrier phase (gas) turbulence as well as the effects of velocity lag between the gas and droplets is also modelled.

Predictions of axial and radial velocity distributions and liquid fractions are found to be realistic. The location of the liquid droplets within the mixing zone is shown to peak away from the oxygen rich center jet. As the turbulent dispersion model for the liquid droplets contains some empirical constants, it is considered important to do some more simulations with a parametric variation of these costants.

Work is in progress to correlate the predictions of this model with experimental results of injection of gas jets into liquid. Unfortunately there is a paucity of data on the liquid particle distributions for such flows. It is hoped that this experimental work will be forthcoming in the near future.

ACKNOWLEDGEMENTS

This work is supported by NOSC IR Program, Project ZW18, under the direction of Dr. Al Gordon.

REFERENCES

1. T.G.Hughes, R.B.Smith and D.H.Kiely: Stored Chemical Energy Propulsion System for Underwater applications, J. of Energy, Vol.7, No.2, March-April 1983, pp128-133.

2. L.P.Cook, E.R.Plante, D.W.bonnell, and J.W.Hastle: High temperature chemistry of stored chemical energy reactions for propulsion, National Bureau of Standards Rept. No.NBSIR 87-3601, July 1987.

3. L.P.Cook and E.R.Plante: Survey of alternate Stored Chemical Energy Reactions, National Bureau of Standards Report No. NBSIR 85-3282, 1985.

4. L.P.Cook, E.R.Plante, R.S.Roth, and J.W.Hastie: Phase equilibria of Stored Chemical Energy Reactants, National Bureau of Standards Report NBSIR 84-2940, 1984.

5. G.M. Faeth: Private communication, 3/1/89.

6. E.Loth & G.M.Faeth: Underexpanded noncondensing turbulent gas jets in liquids, Final report, Aug. 1988, ONR Contract No.N00014-85-0604, Dept of Aerospace Engg., U. of Michigan, Ann Arbor, MI.

7. S.H.Chan etal: Reaction zone structure of gaseous hydrogen chloride jets submerged in aqueous ammonia solutions, Annual Report 9/85-9/86, contract No.N00014-85-k-0752, Dept of Mech Engg., U. of Wisconsin, Milwaukee, WI.

8. D.H.Cho etal: Dynamic behaviour of reacting gas jets submerged in liquids: a photographic study, Rep.ANL-86-41, Argonne National Lab, Argonne, IL.

9. T.Lin & T.Miller: Seminar at NOSC 11/7/88 and personal communication 3/6/89.

10. N.K.Rizk & H.C. Mongia, A model for airblast atomization, AIAA paper 89-2321, AIAA/ASME/SAE/ASEE 25th Joint Propulsion conference, Monterey, CA July 10-12, 1989.

11. P.Y.Liang & M.D. Schuman, Direct numerical simulation of the phase change and heat transfeer of a vaporizing droplet, AIAA paper 89-2432, AIAA/ASME/SAE/ASEE 25th Joint Propulsion conference, Monterey, CA July 10-12, 1989.

12. R.Aggarwal & S. Chitre, Computations of trubulent evaporating sprays, AIAA/ASME/SAE/ASEE 25th Joint Propulsion conference, Monterey, CA, July 10-12, 1989.

13. T.Duvvuri: Two-phase (gas-solid) flow equations for turbulent boundary-layer type flows, AIAA J.,Vol. 5, No. 11, Nov. 1967.

14. T.Duvvuri: Turbulent mixing of gas-particle and pure gas streams in air-augmented rockets, Astronautica Acta, Vol.14, No.6, pp 665-679, Oct. 1969.

15. T.Duvvuri, etal: Mixing, Ignition and Combustion analysis of Air augmented rocket with Boron particles, AIAA J., Vol.7, pp 1581-1587, Aug 1969.

16. L.A.Parnell etal: Radiography of liquid metal fuel combustion, 22nd Intersociety Energy Conversion Engg Conference, Aug.10-14, 1987.

17. E.Mayer: Theory of Atomization in high-velocity gas streams, ARS J., Vol.31, No.12, 1961, p1783.

18. E.Ingebo: Gas density effect on dropsize of simulated fuel sprays, AIAA Paper 89-2322, AIAA/ASME/SAE/ASEE 25th Joint Propulsion Conference, Monterey, CA July 10-12, 1989.

19. J.K.Dukowicz: A particle-fluid numerical model for Liquid Sprays, J. of Computational Physics, Vol 35, pp 229-253, 1980.

20. P.Y.Liang & R.J.Jensen: Modeling of Dense sprays from LOX/Hydrogen Coaxial injectors under supercritical conditions, Proc. 22nd JANNAF Combustion meeting, Oct. 1985.

21. P.Y.Liang & M.Varma: Numerical and experimental studies of atomization and mixing from a coaxial injector element, Porc.23rd JANNAF Combustion meeting, Oct. 1986.

22. A.A.Mostafa and S.E.Elghobashi: Effect of liquid droplets on turbulence in a round gaseous jet, NASA CR-175063, 1986.

23. L.D.Cloutman, J.K.Dukowicz, J.D.Ramshaw, and A.A.Amsden, CONCHAS Spray: A computer code for reactive flows with fuel sprays, Los Alamos National Laboratory, LA-9294-MS, May 1982.

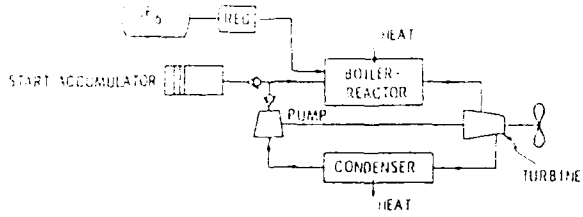

Fig. 1 SCEPS schematic.

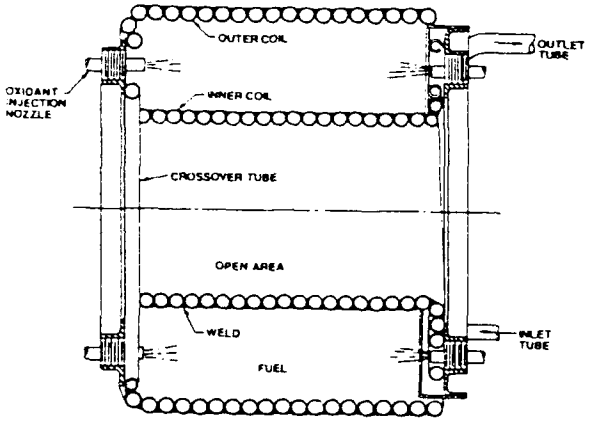

Fig. 2 Boiler reactor schematic.

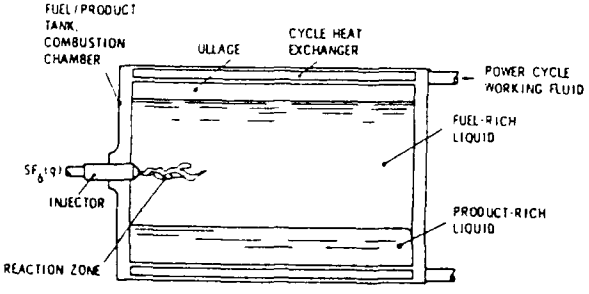

Fig. 3 Batch-type metal combustor.

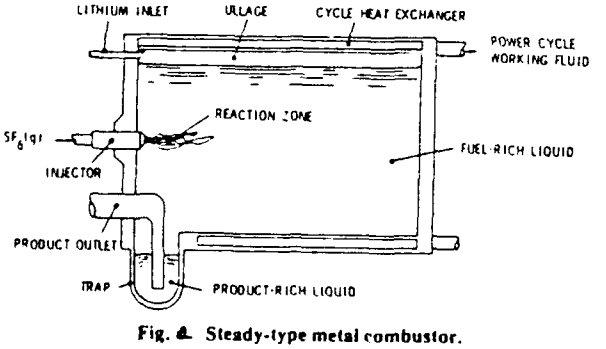

Fig. 4 Steady-type metal combustor.

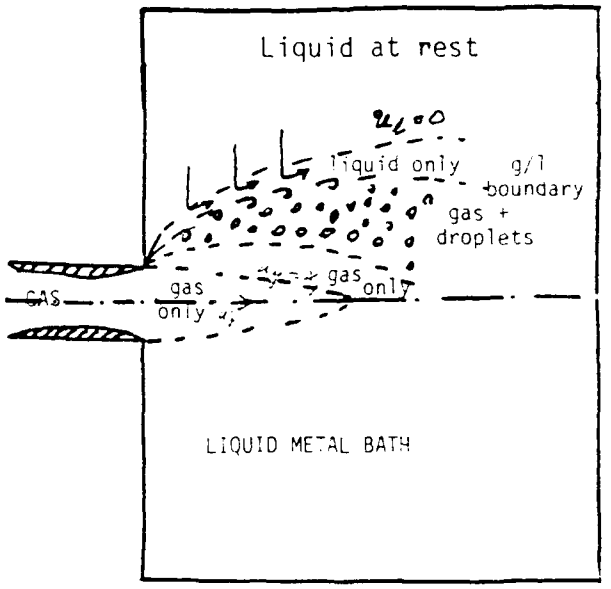

Fig. 5. Schematic of the Flow Field

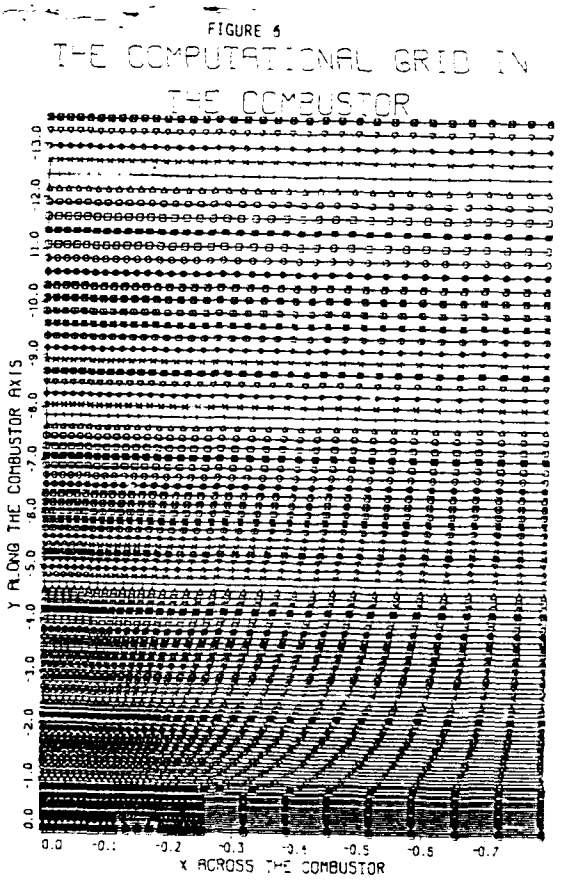

FIGURE 7a

THE GASEOUS AXIAL VELOCTY ACROSS MIXING ZONE

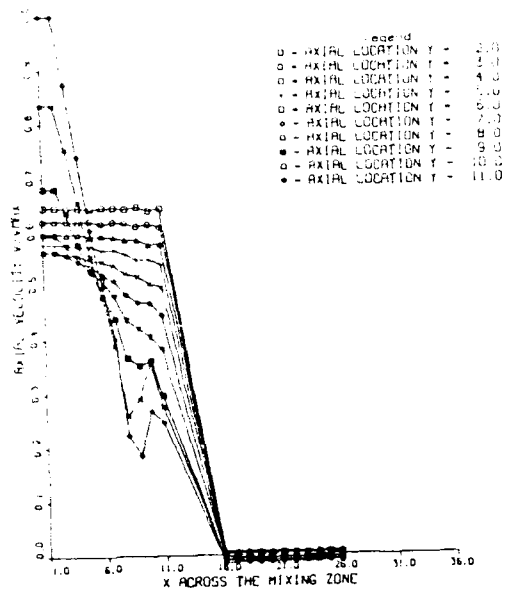

FIGURE 7b

THE GASEOUS AXIAL VELOCTY ACROSS MIXING ZONE

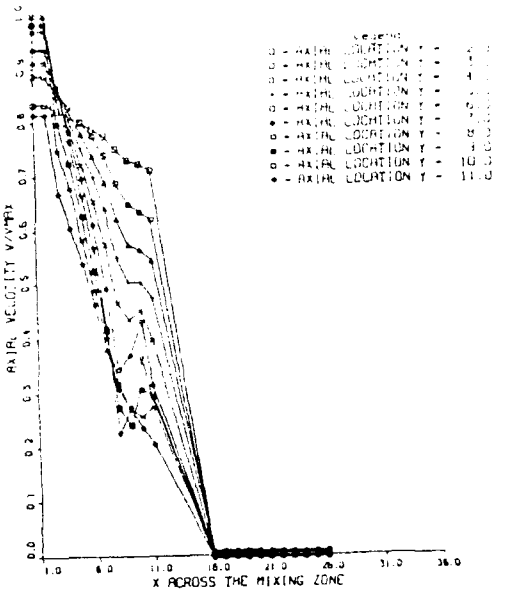

FIGURE 7c

THE GASEOUS AXIAL VELOCTY ACROSS MIXING ZONE

VMAX= 0.811e+05TMAX= 0.478e+03RHOMAX= 0.110e+01

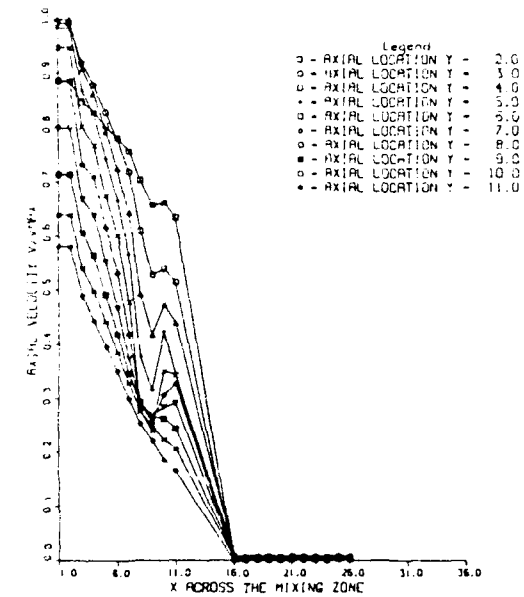

FIGURE 8

THE GASEOUS AXIAL VELOCTY ALONG THE CENTERLINE

VMAX= 0.593e+05cm/secTMAX= 0.828e+03RHOMAX= 0.110e+01

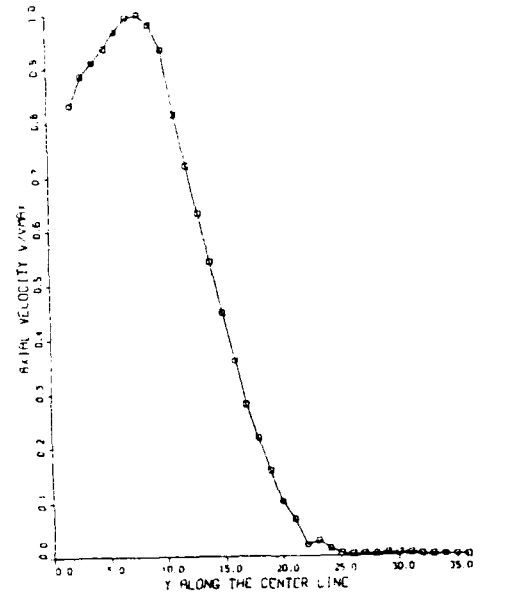

FIGURE 9a

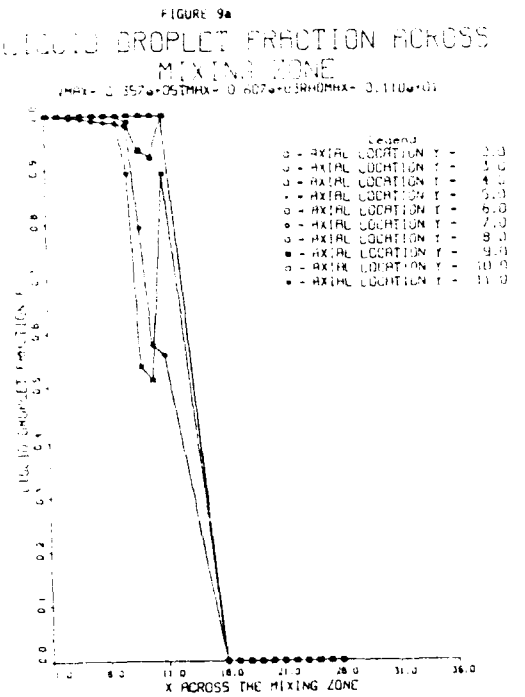

FIGURE 9b

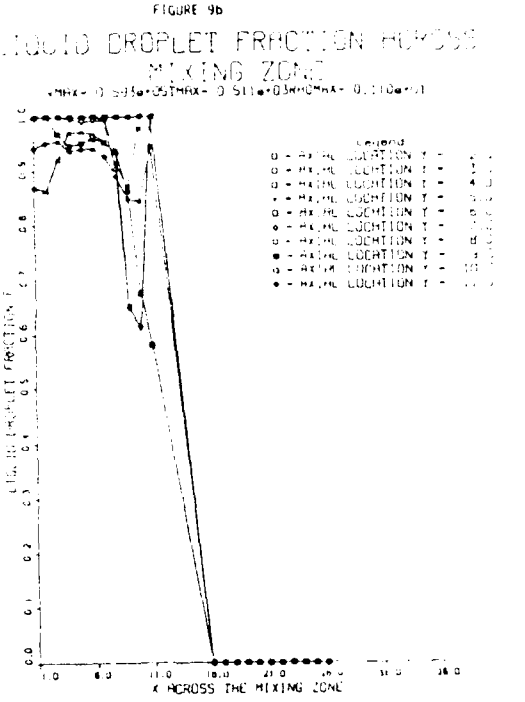

FIGURE 9c

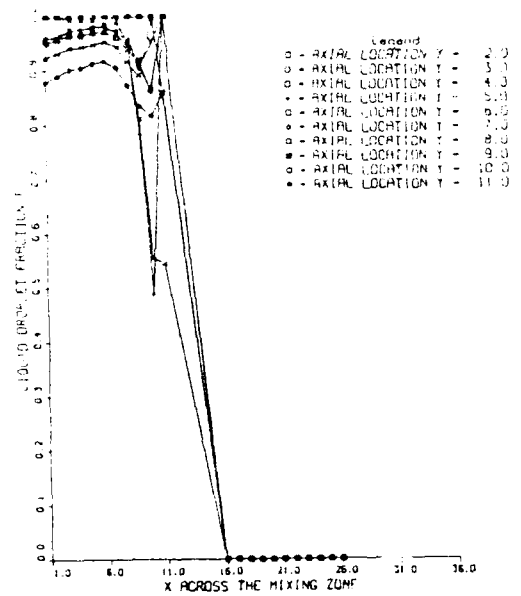

FIGURE 10a

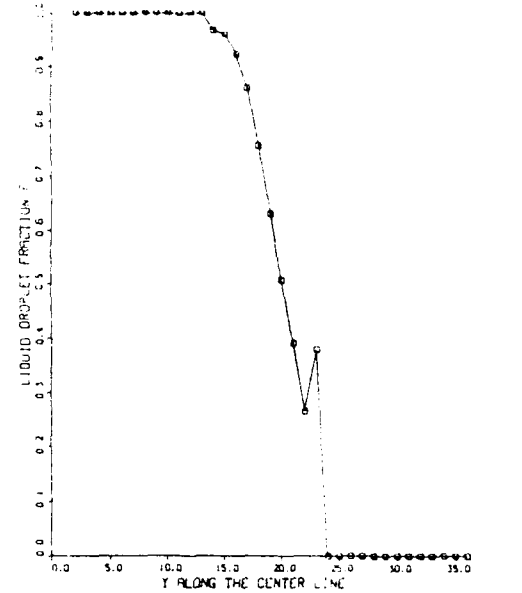

FIGURE 10b

LIQUID DROPLET FRACTION ALONG THE CENTERLINE

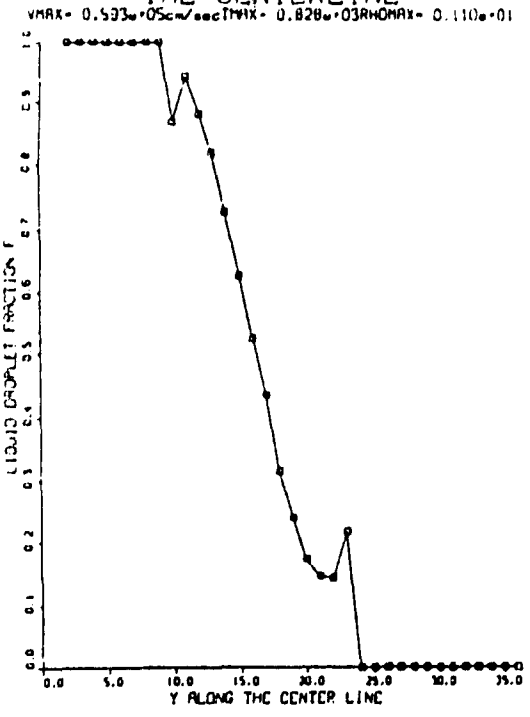

FIGURE 11a

THE LIQUID PARTICLE BOUNDARY ACROSS MIXING ZONE

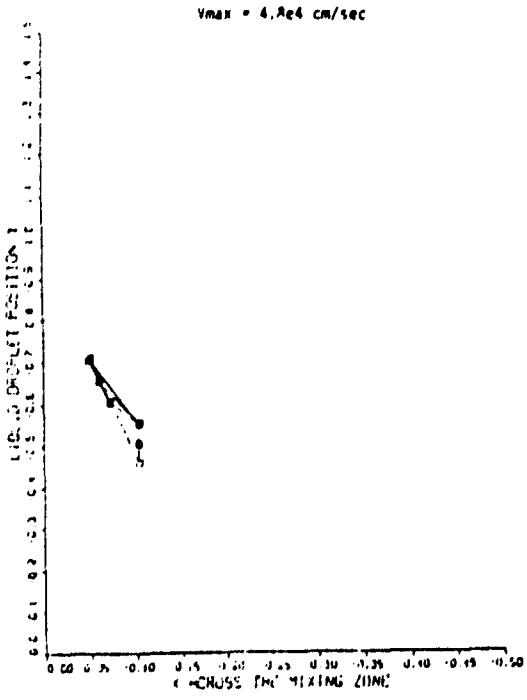

FIGURE 11b

THE LIQUID PARTICLE BOUNDARY ACROSS MIXING ZONE